Taylor & Francis
Taylor & Francis Group

Particulate Science and Technology

An International Journal

ISSN: 0272-6351 (Print) 1548-0046 (Online) Journal homepage: http://www.tandfonline.com/loi/upst20

Discrete element analysis for shear band modes of granular materials in triaxial tests

Hongxiang Tang, Xing Zhang & Shunying Ji

To cite this article: Hongxiang Tang, Xing Zhang & Shunying Ji (2017) Discrete element analysis for shear band modes of granular materials in triaxial tests, Particulate Science and Technology, 35:3, 277-290, DOI: 10.1080/02726351.2016.1153547

To link to this article: http://dx.doi.org/10.1080/02726351.2016.1153547

Accepted author version posted online: 11 Mar 2016.
Published online: 11 Mar 2016.

PARTICULATE SCIENCE AND TECHNOLOGY
2017, VOL. 35, NO. 3, 277–290
http://dx.doi.org/10.1080/02726351.2016.1153547

Taylor & Francis
Taylor & Francis Group

Discrete element analysis for shear band modes of granular materials in triaxial tests

Hongxiang Tang[a], Xing Zhang[a], and Shunying Ji[b]

[a]State Key Laboratory of Coastal and Offshore Engineering, Dalian University of Technology, Dalian, China; [b]State Key Laboratory of Structural Analysis for Industrial Equipment, Dalian University of Technology, Dalian, China

ABSTRACT

The discrete element method (DEM) is adopted to simulate the triaxial tests of granular materials in this study. In the DEM simulations, two different membrane-forming methods are used to generate triaxial samples. One method is to pack the internal particles first, then to generate the enclosed membrane; the other is to generate the internal particles and the enclosed membrane together. A definition of the effective strain, which combines microscopic numerical results with macroscopic expression in three-dimensional space, is presented to describe the macroscopic deformation process of granular materials. With these two membrane generation methods, the effective strain distributions in longitudinal section and transverse section of the triaxial sample are described to investigate the progressive failure and the evolution of the shear bands in granular materials. Two typical shear band failure modes in triaxial tests are observed in the DEM simulations with different membrane-forming methods. One is a single shear band like a scraper bowl, and the other is an axial symmetric shear band like two hoppers stacking as the shape of rotational "X" in triaxial sample. The characteristics of the shear bands during the failure processes are discussed in detail based on the DEM simulations.

KEYWORDS

DEM; effective strain; granular material; shear band; triaxial test

Introduction

Under external loads, the intense deformation of granular materials, such as dense sand, usually occurs in relatively concentrated narrow regions (called shear bands). This phenomenon is also called strain localization and is usually related to the strain-softening property of the material. The mechanism for strain localization and formation of shear bands is an important topic in the study of granular materials.

The shear bands developed in geomaterial are analyzed by experiments and modeled by numerical simulation. Experimental studies of the development and formation of the shear bands are mainly based on triaxial and plane strain tests. The plane strain test is more usually used because the shear band failure is easily triggered and observed in this condition. Vardoulakis (1980) and Desrues et al. (1985) developed plane strain apparatus for this study. Oda, Konishi, and Nemat-Nasser (1982) observed the microstructural changes and development of shear bands in a sand specimen, which provided information about the thickness and direction of shear bands. Zhao and Zhang (2003) modified the true triaxial apparatus to do plane strain tests, which were used to study the development and formation of the shear bands in soils. Sun, Huang, and Yao (2008) used a true triaxial apparatus equipped with three pairs of rigid loading platens to test sand sample under three-dimensional (3D) stress condition. To detect the individual sand grains, and provide detailed particle position and contact maps and calculations of local void ratios, the technique of computed tomography (CT) has been used in the tests for granular materials (Desrues et al. 1996; Alshibli et al. 2000; Oda, Takemura, and Takahashi 2004; Alshibli and Hasan 2008). More recently, based on digital image correlation (DIC) technique, Shao, Wang, and Han (2001) developed and manufactured triaxial apparatus to measure and capture the local deformation appearing on the surface of the soil sample. Nowadays, the technique of DIC is broadly used to directly quantify local displacements on the surfaces of sand specimens throughout plane strain compression (Chupin, Rechenmacher, and Abedi 2011; Rechenmacher, Abedi, and Chupin 2010; Rechenmacher et al. 2011). Combining the techniques of CT and DIC, the initial, spatial, mesoscale parameter variation in the specimen as well as the specimen deformation fields before and after localization can be measured (Hall et al. 2010; Borja et al. 2013).

Generally speaking, the shear band modes occurring in ordinary triaxial test are very complicated and difficult to be captured because most part of the shear bands locate in the interior part of the sample and keep unseen. In this condition, numerical simulation, combined with experiments, may be the efficient way to study the development of the shear bands.

To illustrate the mechanics of shear bands, the discrete element method (DEM) is used to analyze and simulate the triaxial test of granular material. Granular material is an assembly of discrete particles which are in contact with each other at a microscopic level. It has been recognized that microstructure properties, such as particle packing style, distribution of void ratios, and their evolution, control the macroscopic

CONTACT Hongxiang Tang tanghx@dlut.edu.cn No. 2 Linggong Road, Ganjingzi District, Dalian City, Liaoning Province, P.R.C., 116024.
Color versions of one or more of the figures in the article can be found online at www.tandfonline.com/upst.

behavior of granular materials. The DEM has been widely used to investigate the failure micro-mechanism of granular materials because of its ability to obtain the microscopic information at the particle level (Cundall and Strack 1979; Chang and Misra 1988; Zhang and White 1998; Oda and Kazama 1998; Oda and Iwashita 1999). DEM allows for a contact model between two particles, viz. force−displacement law, to calculate the contact force. The physical properties and relative motion mechanism of particles in granular material are reflected by the contact models between particles. Using different contact models, different macroscopic behaviors can be achieved with DEM (Al-Raoush 2007; Kozicki and Donze 2009; Abe, Van, and Urai 2011; Hare and Ghadiri 2013). Also, DEM is used to model the triaxial tests. Belheine et al. (2009) simulated the ordinary triaxial test with 3D DEM in which the roughness of grains was taken into account. Using a 3D spherical discrete model with a rolling resistance, Christophe, Philippe, and Pascal (2009) modelled the triaxial test to study the influence of relative density on granular materials behavior.

Compared with the rigid boundary usually utilized in DEM, the flexible boundary can reflect the localized deformation phenomena better, and explain the overall macroscopic mechanical behavior of geomaterials from the view of mesoscopic particles (Geraldine and Catherine 2008). This paper imitates lateral membrane of the triaxial sample as a flexible boundary of the numerical model. Based on a widely used and commercially available 3D DEM code, PFC3D, two methods are used to generate the particles and the membrane for triaxial sample: one is to generate the internal particles first, then to generate the enclosed membrane; the other is to generate them at the same time.

To understand and describe the macroscopic deformation process and the evolution of shear bands in granular material, a macroscopic definition of effective strain, which combines microscopic numerical results with macroscopic expression in 3D space, is presented. With these methods, the mechanical behavior of granular materials in triaxial test is studied, and two typical shear band failure modes are obtained.

Discrete element method and definition of effective strain for granular material

Introduction of the DEM

The DEM used in the present study is described in Figure 1. The normal contact force, the tangential contact force between particles in contact are computed as

$$\begin{cases} F_{\mathrm{n}} = k_{\mathrm{n}} U_{\mathrm{n}} + c_{\mathrm{n}} \frac{dU_{\mathrm{n}}}{dt} \\ F_{\mathrm{t}} = \min(k_{\mathrm{s}} U_{\mathrm{s}} + c_{\mathrm{s}} \frac{dU_{\mathrm{s}}}{dt}, \mu_{\mathrm{s}} |F_{\mathrm{n}}|) \end{cases}, \tag{1}$$

where F_{n} is the normal contact force; F_{t}, the tangential contact force; k_{n}, the stiffness coefficient of normal force; k_{s}, the stiffness coefficient of sliding force; U_{n}, the normal displacement; U_{s}, the tangential sliding displacement; c_{n}, the viscous damping coefficient of normal force; c_{s}, the viscous damping coefficient of sliding force; and μ_{s}, the sliding friction force coefficient.

Definition of effective strain of granular materials

In order to understand the microscopic mechanism of the mechanical response of granular materials, and describe the macroscopic deformation process of granular materials, this paper attempts to combine microscopic numerical experiments with macroscopic expression and presents a definition of the effective strain of granular material in three dimensions, which is used to analyze the evolution of shear band and strain localization in triaxial test.

There are many strain definitions, such as the best-fit strains (Liao et al. 1997) and the strains defined on the basis of an equivalent continuum (Bagi 1996). Based on the changes of the center location of the particles, a nominal effective strain was used to measure the relative change of location between the particle and its surrounding particles in two dimensions (Li et al. 2005). In this study, the definition of effective strain is extended to 3D conditions. The nominal effective strain defined in three dimensions is as follows.

As is shown in Figure 2, consider the position change of two neighboring particles during the time-step from t_1 to t_2. Referring to the global coordinates, the center coordinates of the particles A and B are $\mathbf{X}_{\mathrm{A}}^1$, $\mathbf{X}_{\mathrm{B}}^1$ in t_1 and $\mathbf{X}_{\mathrm{A}}^2$, $\mathbf{X}_{\mathrm{B}}^2$ in t_2, respectively. The angles between the axis of X, Y, Z in global coordinate and the corresponding local coordinates are α_1, β_1, γ_1 in t_1 and α_2, β_2, γ_2 in t_2, respectively.

Referring to global coordinates, the difference between the center position of particles A and B in t_1 and t_2

$$\Delta\mathbf{X}_{\mathrm{BA}}^1 = \mathbf{X}_{\mathrm{B}}^1 - \mathbf{X}_{\mathrm{A}}^1;\ \Delta\mathbf{X}_{\mathrm{BA}}^2 = \mathbf{X}_{\mathrm{B}}^2 - \mathbf{X}_{\mathrm{A}}^2. \tag{2}$$

Referring to local coordinate system,

$$\Delta\mathbf{x}_{\mathrm{BA}}^1 = \mathbf{x}_{\mathrm{B}}^1 - \mathbf{x}_{\mathrm{A}}^1;\ \Delta\mathbf{x}_{\mathrm{BA}}^2 = \mathbf{x}_{\mathrm{B}}^2 - \mathbf{x}_{\mathrm{A}}^2. \tag{3}$$

By coordinate transformation system,

$$\Delta\mathbf{x}_{\mathrm{BA}}^1 = \mathbf{T}_1 \Delta\mathbf{X}_{\mathrm{BA}}^1;\ \Delta\mathbf{x}_{\mathrm{BA}}^2 = \mathbf{T}_2 \Delta\mathbf{X}_{\mathrm{BA}}^2. \tag{4}$$

The local coordinate system can be rotated β'_1 radian circling y_1 direction, then rotated γ'_1 radian circling z_1 direction, so as to coincide with the direction of the global coordinate system in t_1. Similarly, the local coordinate system can be rotated β'_2 radian circling y_2 direction, then rotated γ'_2 radian circling z_2 direction, so as to coincide with the direction of the global coordinate system in t_2. The coordinate transformation matrixes from the local coordinate system to the global coordinate system are $\mathbf{T}_1$ in t_1 and $\mathbf{T}_2$ in t_2, respectively.

$$\mathbf{T}_1 = \begin{bmatrix} \cos\gamma'_1 & \sin\gamma'_1 & 0 \\ -\sin\gamma'_1 & \cos\gamma'_1 & 0 \\ 0 & 0 & 1 \end{bmatrix} \begin{bmatrix} \cos\beta'_1 & 0 & -\sin\beta'_1 \\ 0 & 1 & 0 \\ \sin\beta'_1 & 0 & \cos\beta'_1 \end{bmatrix}, \tag{5}$$

$$\mathbf{T}_2 = \begin{bmatrix} \cos\gamma'_2 & \sin\gamma'_2 & 0 \\ -\sin\gamma'_2 & \cos\gamma'_2 & 0 \\ 0 & 0 & 1 \end{bmatrix} \begin{bmatrix} \cos\beta'_2 & 0 & -\sin\beta'_2 \\ 0 & 1 & 0 \\ \sin\beta'_2 & 0 & \cos\beta'_2 \end{bmatrix}. \tag{6}$$

Deformation gradient f is used to describe the relative location change between particles A and B, for which the polar decomposition is written as

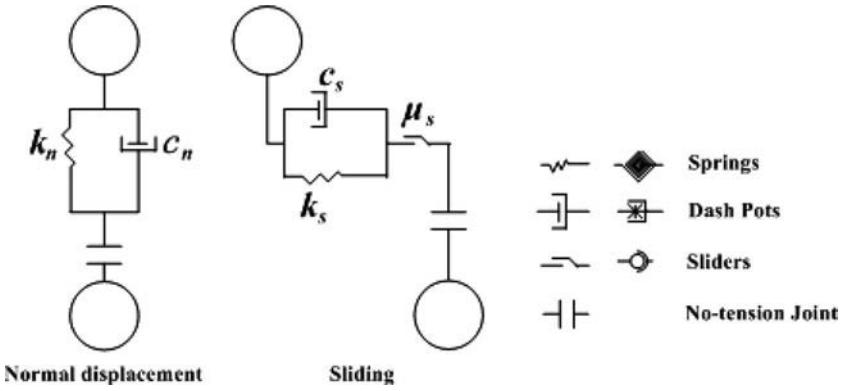

Figure 1. The contact model used in DEM.

$$f = \frac{\Delta \mathbf{x}^2_{\mathrm{BA}}}{\Delta \mathbf{x}^1_{\mathrm{BA}}} = \mathbf{RU}. \tag{7}$$

In Equation (7), **R** is the orthogonal tensor, which represents the rotation of the connecting line between particles *A* and *B*; and **U** is a positive definite symmetric tensor, which represents the tensile deformation of the connecting line between particles *A* and *B*. Here, we have

$$\mathbf{R} = \begin{bmatrix} \cos\gamma'_1 & \sin\gamma'_1 & 0 \\ -\sin\gamma'_1 & \cos\gamma'_1 & 0 \\ 0 & 0 & 1 \end{bmatrix} \begin{bmatrix} \cos(\beta'_2-\beta'_1) & 0 & \sin(\beta'_2-\beta'_1) \\ 0 & 1 & 0 \\ -\sin(\beta'_2-\beta'_1) & 0 & \cos(\beta'_2-\beta'_1) \end{bmatrix} \begin{bmatrix} \cos\gamma'_2 & -\sin\gamma'_2 & 0 \\ \sin\gamma'_2 & \cos\gamma'_2 & 0 \\ 0 & 0 & 1 \end{bmatrix}, \tag{8}$$

$$\mathbf{U} = \begin{bmatrix} \lambda_{\mathrm{AB}} & 0 & 0 \\ 0 & 1 & 0 \\ 0 & 0 & 1 \end{bmatrix}, \tag{9}$$

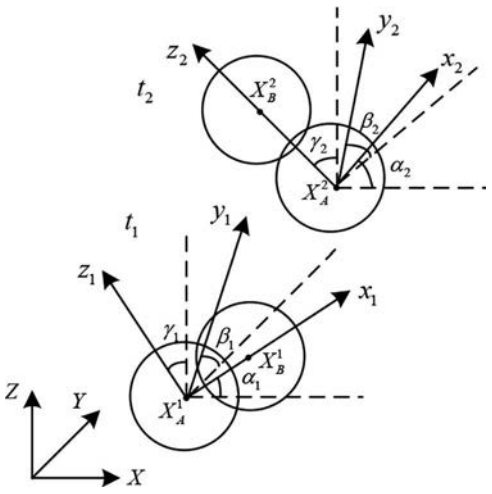

Figure 2. The position of neighboring particles at different time.

Figure 3. Two typical shear band patterns of soil in triaxial shear tests: (a) "X" shear band pattern; (b) single shear band pattern.

$$\begin{cases} \frac{\lambda_{\mathrm{AB}}=l_{\mathrm{AB}}{}^2}{l^1_{\mathrm{AB}}} \\ l^1_{\mathrm{AB}} = \left\|\Delta \mathbf{x}^1_{\mathrm{BA}}\right\| \\ l^2_{\mathrm{AB}} = \left\|\Delta \mathbf{x}^2_{\mathrm{BA}}\right\| \end{cases}, \tag{10}$$

where || means the modulus of a vector.

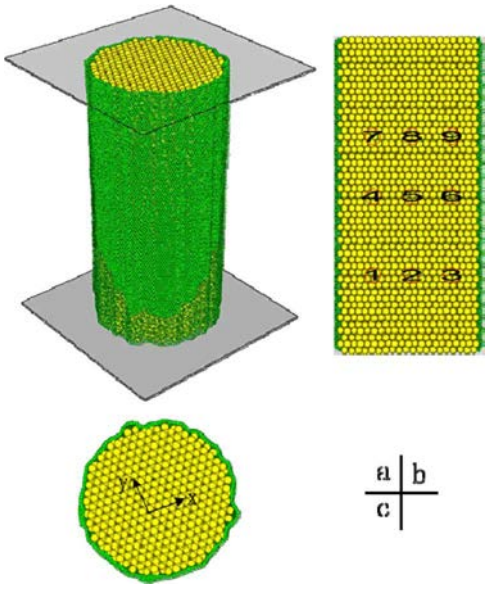

Figure 4. The numerical model for the triaxial compression test.

Table 1. The basic parameters for the numerical simulation of triaxial test.

	Particle size (mm)	Particle density (g/cm^3)	Coefficient of friction	Normal stiffness (MN/m)	Tangential stiffness (MN/m)	Normal contact strength (N/m)	Tangential contact strength (N/m)
Internal specimen	2.0	2.65	0.25	2.0	2.0	0	0
Membrane structure	0.8	2.65	0.0	0.02	0.02	100.0	100.0
Wall	—	—	0.0	25.0	25.0	—	—

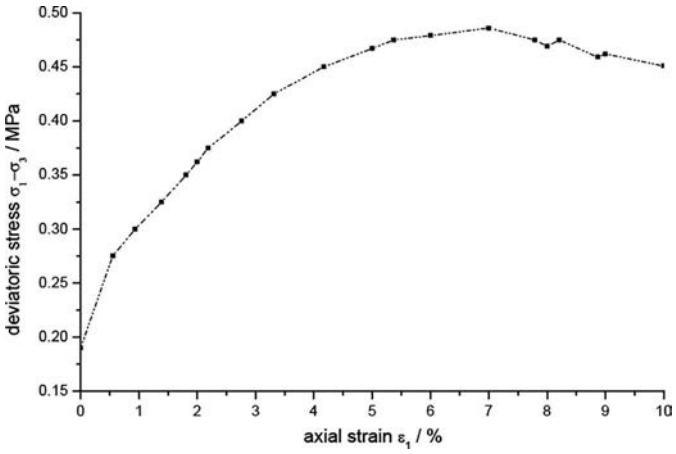

Figure 5. The deviatoric stress–axial strain curves for the triaxial compression test.

From Equations (4)–(7), we have,

$$\begin{cases} \Delta \mathbf{X}_{\mathrm{BA}}^{2} = \mathbf{F}\Delta \mathbf{X}_{\mathrm{BA}}^{1} \\ \mathbf{F} = \mathbf{T}_{2}^{\mathrm{T}}\mathbf{f}\mathbf{T}_{1} \end{cases} . \tag{11}$$

According to continuum mechanics, the derivative tensor of displacement gradient defined by the relationship between material coordinate and space coordinate is

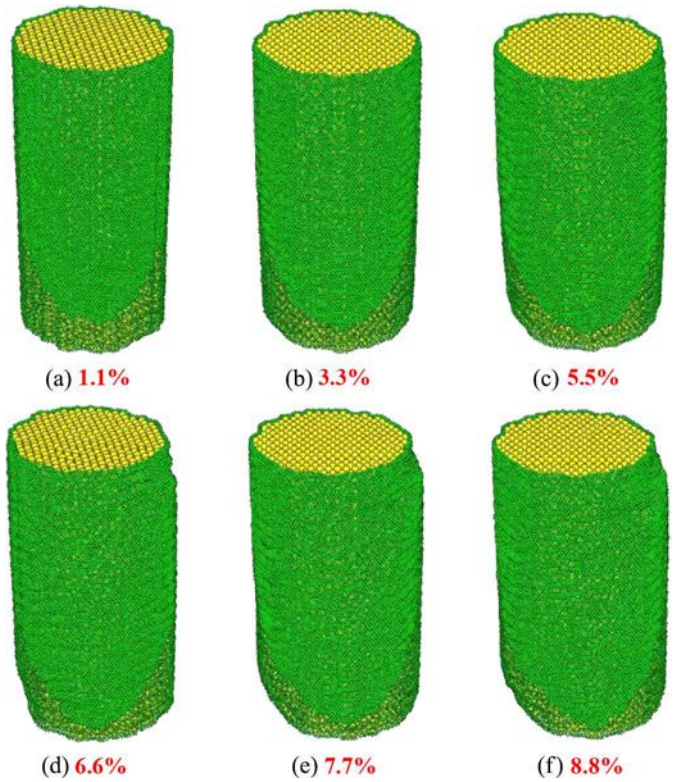

Figure 6. The deformation of the triaxial compression specimen at different axial strains.

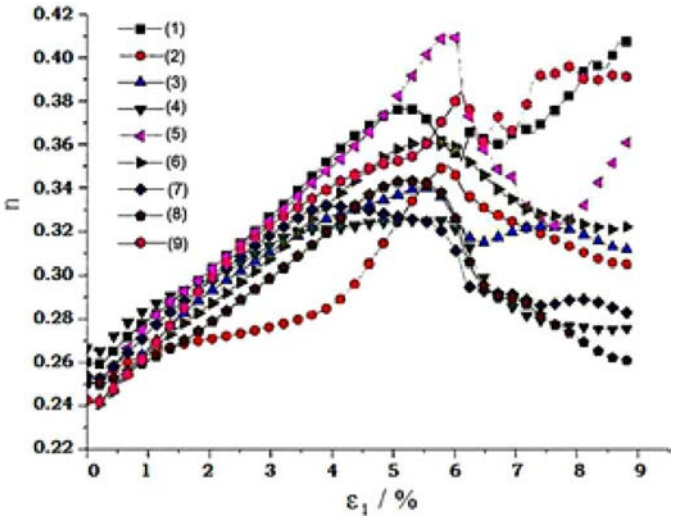

Figure 7. The changes of porosity of the measurement balls in the triaxial test.

$$\mathbf{D} = \mathbf{F} - \mathbf{I}, \tag{12}$$

where $\mathbf{I}$ is unit matrix. If D_{ij} is the component of $\mathbf{D}$, then

$$\gamma_{\mathrm{AB}} = \left[\frac{2}{3}D_{ij}D_{ij}\right]^{1/2}, \tag{13}$$

$$\gamma_{\mathrm{e}} = \frac{1}{n_{\mathrm{A}}}\sum_{B=1}^{n_{\mathrm{A}}}\gamma_{\mathrm{AB}}, \tag{14}$$

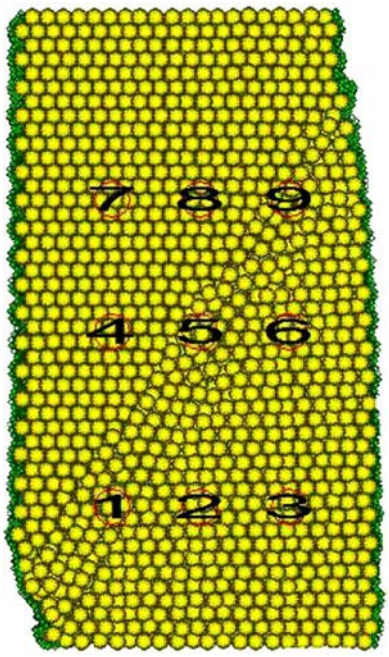

Figure 8. The positions of the particles at the axial strain of 8.8% in vertical section of the specimen.

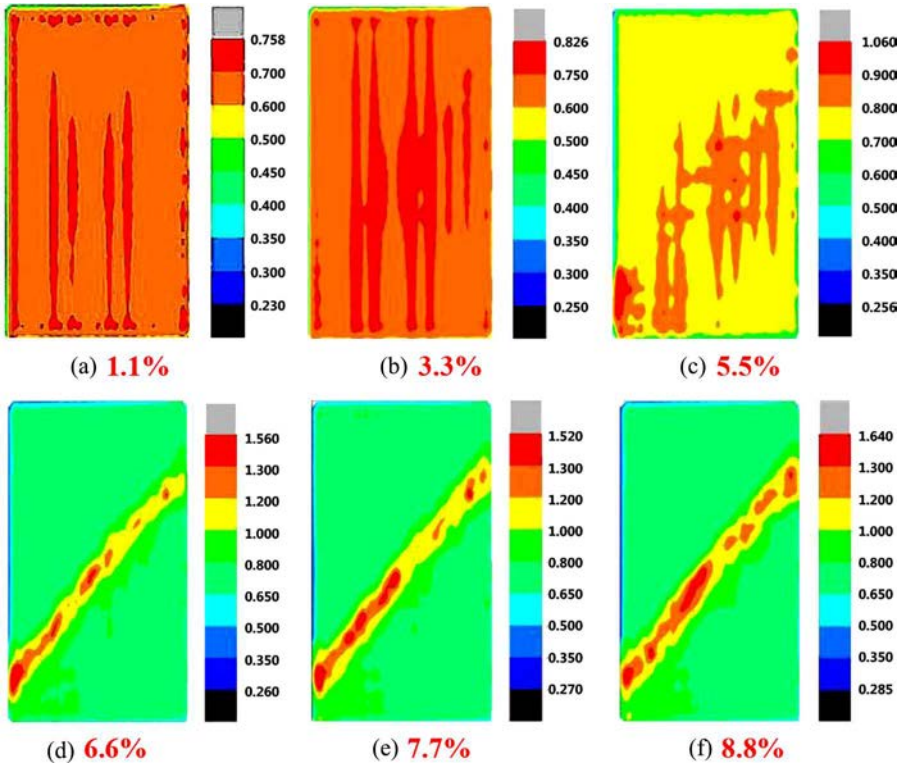

Figure 9. The effective strain distributions in the vertical section (*x*-direction) of the triaxial compression specimen at different axial strains.

where γ_{AB} is an intermediate variable, and γ_e is the effective strain of particle A, around which there are n_A neighboring particles.

The definition of effective strain, which is easily understood and acceptable from macro-scope for granular assembly, is introduced to intuitively exhibit the development process of shear bands in the next parts of this paper.

Generation of triaxial specimen and enclosed membrane of granular materials

In the discrete element method, it is very important to generate the membrane particles in simulating triaxial tests. To simulate the evolution of shear bands in triaxial tests based on discrete element method, two methods of particles generation can be used (Geraldine and Catherine 2008).

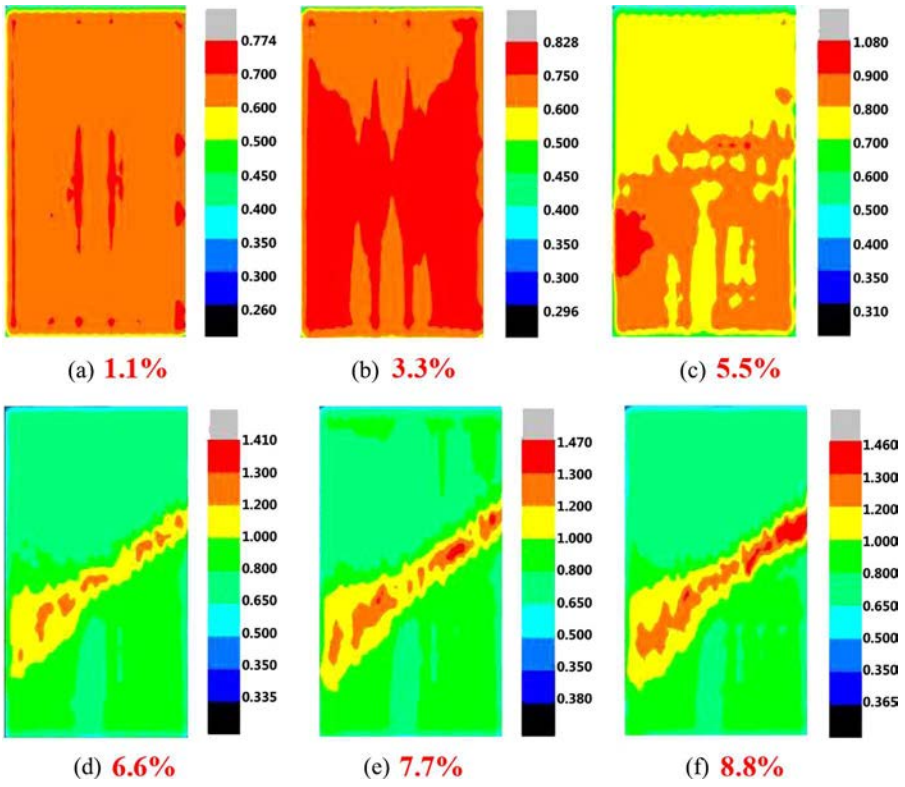

Figure 10. The effective strain distributions in the vertical section (*y*-direction) of the triaxial compression specimen at different axial strains.

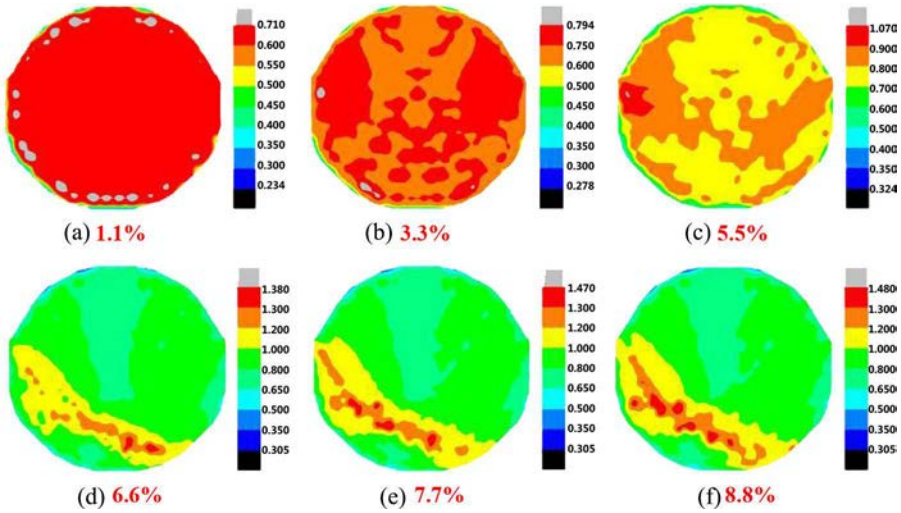

Figure 11. The effective strain distributions in the cross section (*z*-direction) at the place of 1/4 height of the specimen at different axial strains.

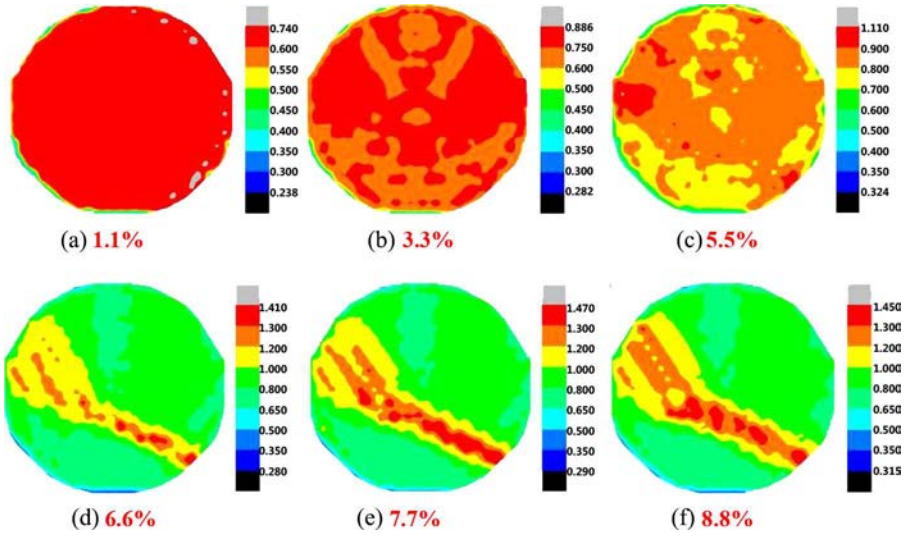

Figure 12. The effective strain distributions in the cross section (*z*-direction) at the place of 3/8 height of the specimen at different axial strains.

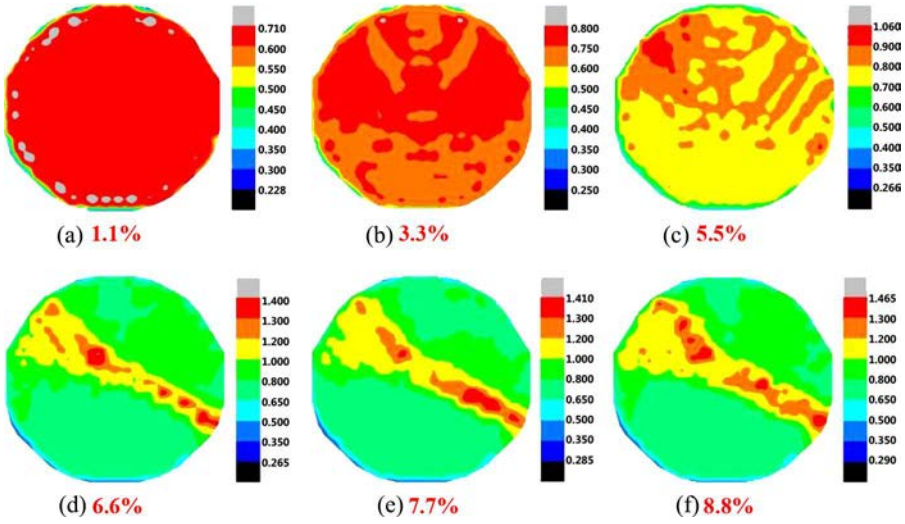

Figure 13. The effective strain distributions in the cross section (*z*-direction) at the place of 1/2 height of the specimen at different axial strains.

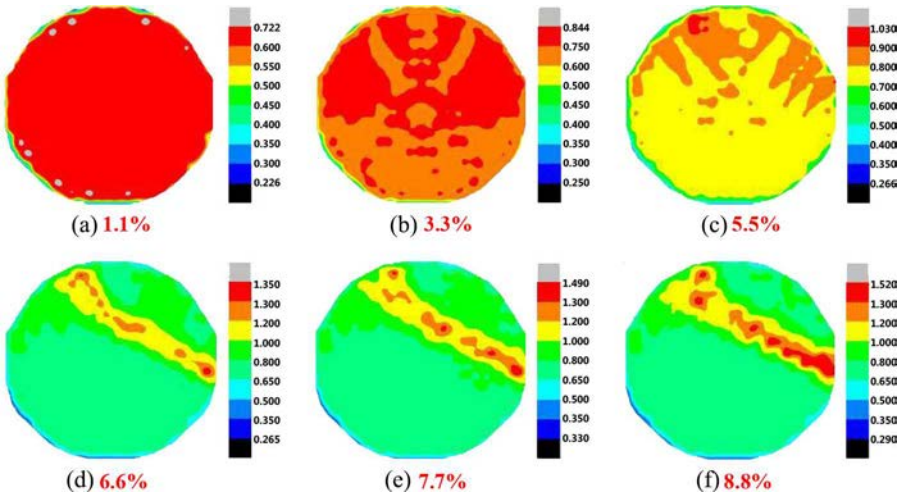

Figure 14. The effective strain distributions in the cross section (*z*-direction) at the place of 5/8 height of the specimen at different axial strains.

One method is to generate the particles of internal specimen and enclosed membrane independently, while the particles of membrane are smaller than those of internal specimen. This method is called the "step-by-step membrane-forming method." Another method is to generate the particles of the internal specimen and the enclosed membrane at the same time, but the properties of the outmost particles of the specimen are set as those of the membrane. This method is named as "once membrane-forming method." With these two particle generation methods above, we investigate the progressive failure and the evolution of the shear bands in triaxial tests with DEM simulation, and the effects of particle generation methods on the patterns of shear bands in the triaxial specimens. In fact, it will be found that the results based on these two methods represent two typical failure modes, which are usually encountered in triaxial tests in laboratory, as shown in Figure 3.

Failure mode analysis of shear band in triaxial test

Discrete element simulation with step-by-step membrane-forming method of triaxial test

The specimen of triaxial test has a cylindrical structure with the height of 80.5 mm and the diameter of 38 mm. First, 14,064 particles with diameter of 2 mm and the porosity of 0.2595 are generated to form the internal specimen. Then, the particles with diameter of 0.8 mm in the outmost layer of the specimen are generated as the membrane structure. Rigid plates, on which the compression forces will be applied, are set on the top and bottom of the specimen, as shown in Figure 4a. The whole discrete element model of the triaxial test is illustrated in Figure 4, where "a" is the view of overall specimen; "b" is the view of vertical section of the specimen, where the digits $1-9$ are the numbers of measurement ball arranged; and "c" is the view of transverse section of the specimen. The material parameters used in the analysis are presented in Table 1.

A confining pressure of 0.2 MPa is imposed on the internal specimen through the membrane structure. The membrane structure is composed of the particles in the outermost layer of the specimen. According to Geraldine and Catherine (2008), the confining pressure can be applied on individual particles in the membrane region.

During the compressing process, the confining pressure is constant, and the compression load is applied continuously by displacement control of the rigid plates, which are forced to move toward each other vertically. To describe the numerical results of the granular specimen during this process,

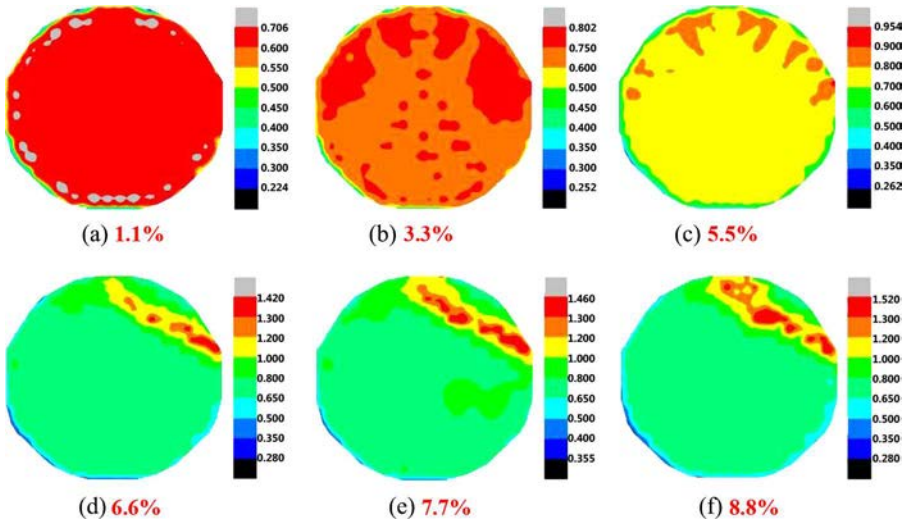

Figure 15. The effective strain distributions in the cross section (*z*-direction) at the place of 3/4 height of the specimen at different axial strains.

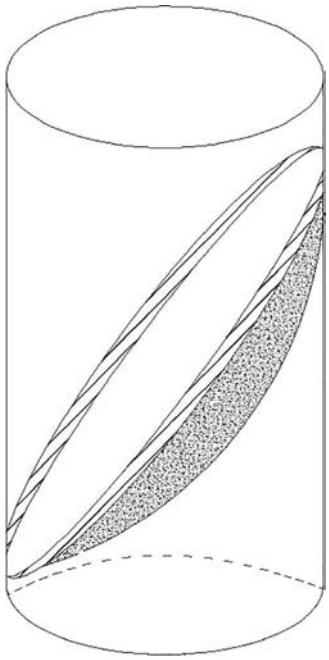

Figure 16. The outline of the shear band in triaxial test.

the deformation of the specimen, porosities of measurement balls, and effective strain distributions in the specimen are presented.

Figure 5 gives the curve of axial deviatoric stress−strain for the specimen, which illustrates that a peak axial stress value of 0.487 MPa arrives at axial strain of 7%, then a softened axial stress−strain curve appears. Figure 6 gives the deformation of the specimen at different axial strains. It can be seen that deflexion of the specimen occurs after the axial strain of 5.5%. Porosities of measurement balls at various axial strains

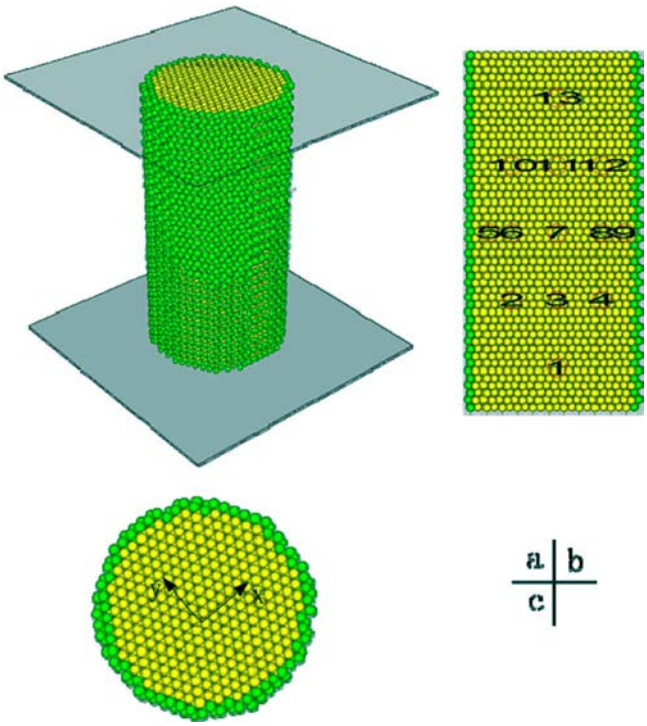

Figure 17. The numerical model for the triaxial compression test.

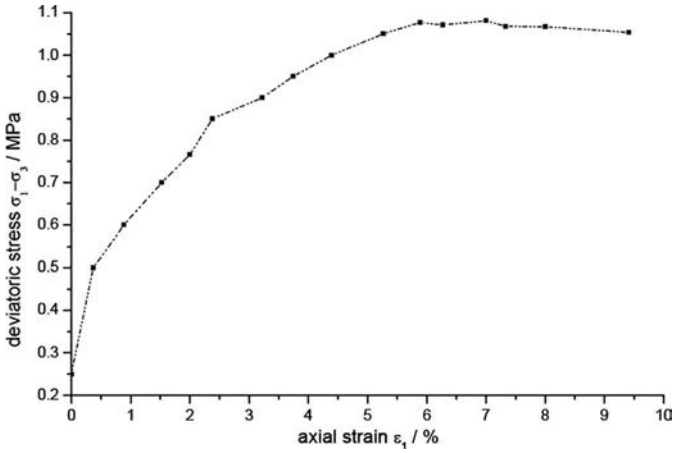

Figure 18. The axial deviatoric stress−strain curve for the triaxial compression test.

are illustrated in Figure 7, where the porosities of the measurement balls (1), (5), and (9) are significantly greater than those of the other measurement balls near the axial strain of 5.5%. Figure 8 gives the positions of the particles at the axial strain of 8.8% in vertical section of the specimen, which shows that the relative movements of the particles and the deformation of the specimen are mainly concentrated in a diagonal shear band, while the positions of particles in other parts of the specimen change little. It also can be seen that the measurement balls (1), (5), and (9) are just located in the diagonal shear band.

To better understand the progressive development and spatial distribution of the shear band in triaxial compression specimen under this condition, Figures 9–15 give the effective strain distributions along x-direction and y-direction in the vertical sections, respectively, and at different heights of the triaxial specimen in the transverse sections with increasing axial strains.

Figure 9 gives the effective strain distributions along x-direction in the vertical section of the triaxial specimen with increasing axial strains. Figure 10 gives the effective strain distributions along y-direction in the vertical section of the triaxial specimen with increasing axial strains. It can be seen that a diagonal shear band develops distinctly after the axial strain of 5.5% and runs through the triaxial specimen progressively in these two directions.

Figures 11–15 give the effective strain distributions in the cross section along z-direction at the heights of $2/8h$, $3/8h$, $4/8h$, $5/8h$, and $6/8h$ (h is the height of the triaxial specimen) of the triaxial specimen, respectively, with increasing axial strains. It can be seen that the shear band develops not only in these cross sections distinctly after the axial strain of 5.5% but also in different parts for different cross sections, namely from one side of the cross section to the middle and then to the other side of the cross section as the height of the cross section increases.

According to the effective strain distributions in the vertical sections and cross sections above, the sketch of a complete shear band like a scraper bowl which originates from the upper triaxial specimen and slants through the sample can be figured out, as is shown in Figure 16.

Table 2. The basic parameters for the numerical simulation of triaxial test.

	Particle size (mm)	Particle density (g/cm^3)	Coefficient of friction	Normal stiffness (MN/m)	Tangential stiffness (MN/m)	Normal contact strength (N/m)	Tangential contact strength (N/m)
Internal specimen	2.0	2.65	0.25	2.0	2.0	0	0
Membrane structure	2.0	2.65	0.0	0.02	0.02	100.0	100.0
Wall	—	—	0.0	25.0	25.0	—	—

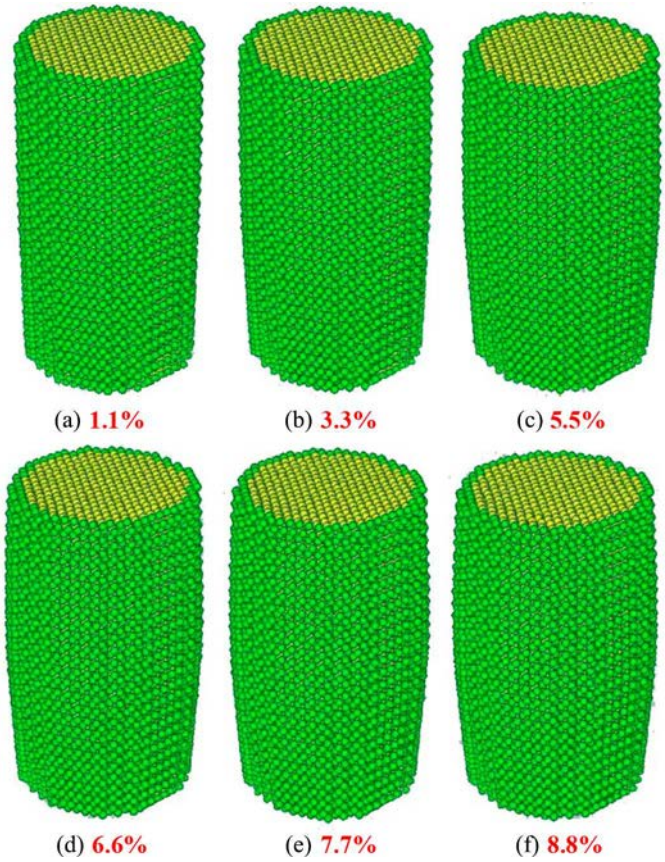

Figure 19. The deformation of particle sample for the triaxial compression test.

From the analysis above, it can be concluded that the development of shear band starts before the peak value of stress and that the deformation is mainly concentrated in a diagonal shear band while the other parts of the specimen have less deformation.

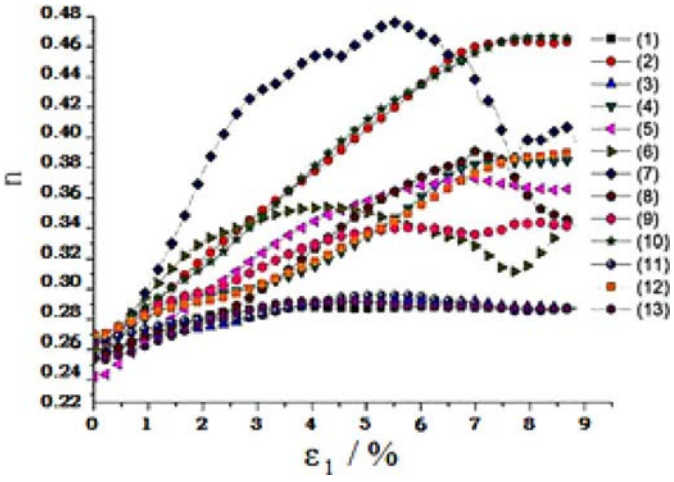

Figure 20. The porosity changed in the measure spheres of granular sample.

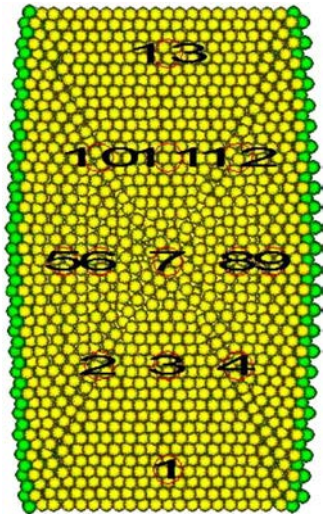

Figure 21. The positions of the granules at the axial strain of 8.8% in the vertical section of sample.

Discrete element simulation with once membrane-forming method of triaxial test

The specimen of triaxial test has a cylinder structure with the height of 80.5 mm and the diameter of 40 mm. Total 168,54 particles with diameter of 2 mm and the porosity of 0.2595 are generated in the specimen, where the outmost green layer are set as the membrane structure, as can be seen in Figure 17, where "a" is the view of overall specimen; "b" is the view of vertical section of the specimen, where the digits 1–13 are the numbers of measurement ball arranged; and "c" is the view of transverse section of the specimen. The boundary and loading conditions are the same as that of Figure 4. The material parameters used in the analysis are presented in Table 2.

A confining pressure of 0.2 MPa, which is constant during the compressing process, is imposed on the internal specimen through the enclosed membrane. The rigid plates are forced to move toward each other vertically by displacement control. During the compression process, the deformation of the specimen, the porosities of measurement balls, and the effective strain distributions in the specimen are analyzed.

The curve of axial deviatoric stress−strain for the specimen is given in Figure 18, which illustrates that a peak axial deviatoric stress value of 1.08 MPa arrives at axial strain of 6.8%, followed by a little soften stress−strain curve. The peak stress is greater than previous one as the constraints of the membrane boundary in this case are stronger.

The deformation of the specimen at different axial strains is given in Figure 19. It cannot be seen that the deformation localizes in the inner specimen but that swelling of the middle of specimen occurs after the axial strain of 5.5%. Figure 20 gives the porosities of measurement balls at various axial strain, which illustrates that the porosities of the measurement balls

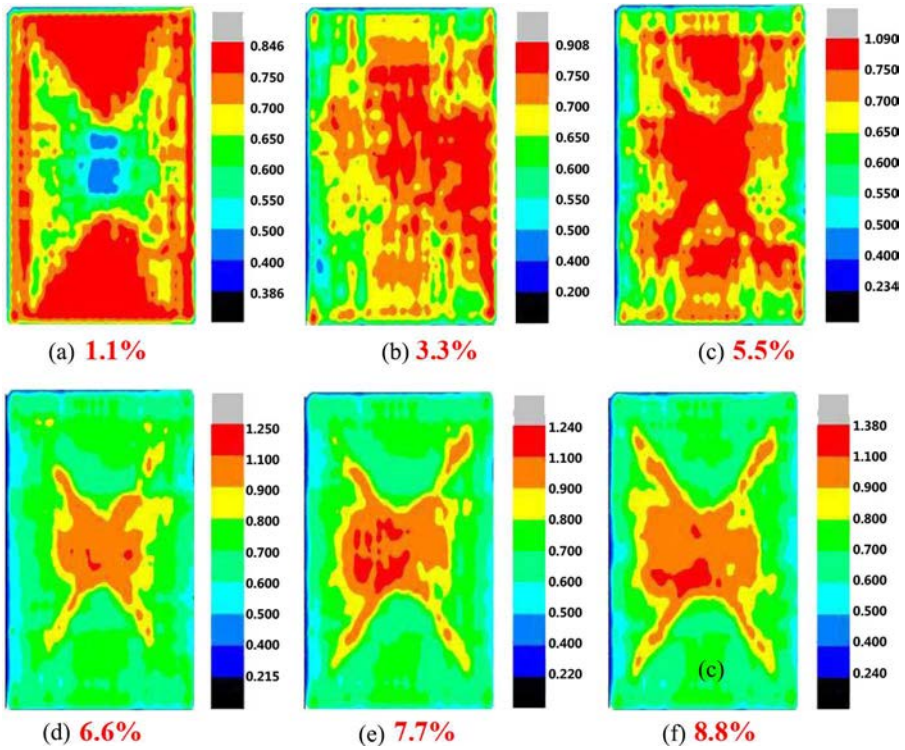

Figure 22. The effective strain distributions in the vertical section (*x*-direction) of granular assembly with increasing vertical displacements.

(2), (7), and (10) are significantly greater than those of the other measurement balls near the axial strain of 5.5%, while the porosities of the measurement balls (1), (3), (11), and (13) are very less than others. Figure 21 gives the positions of the particles at the axial strain of 8.8% in vertical section of the specimen, which shows that the relative movements of the particles and the deformation of the specimen are mainly concentrated in two intersection shear bands like the shape of "X" while the positions of particles in other parts of the specimen change little. It also can be seen that the measurement balls (2), (7), and (10) are just located in the shear bands.

In this case, the progressive development and spatial distribution of the shear band in triaxial compression specimen can be seen from Figures 22–28, which give the effective strain

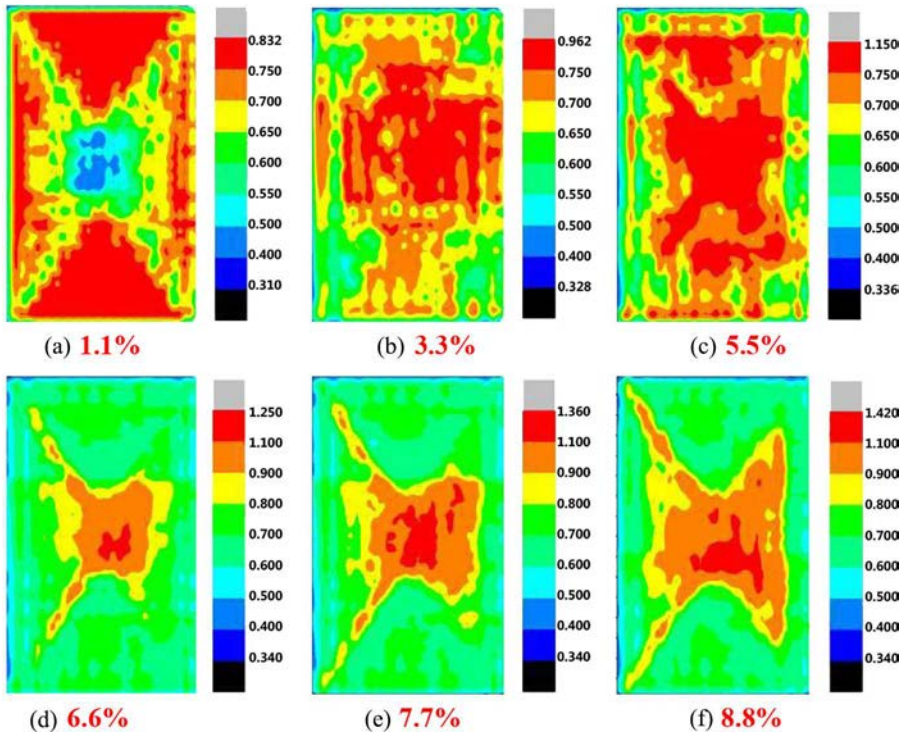

Figure 23. The effective strain distributions in the vertical section (*y*-direction) of granular assembly with increasing vertical displacements.

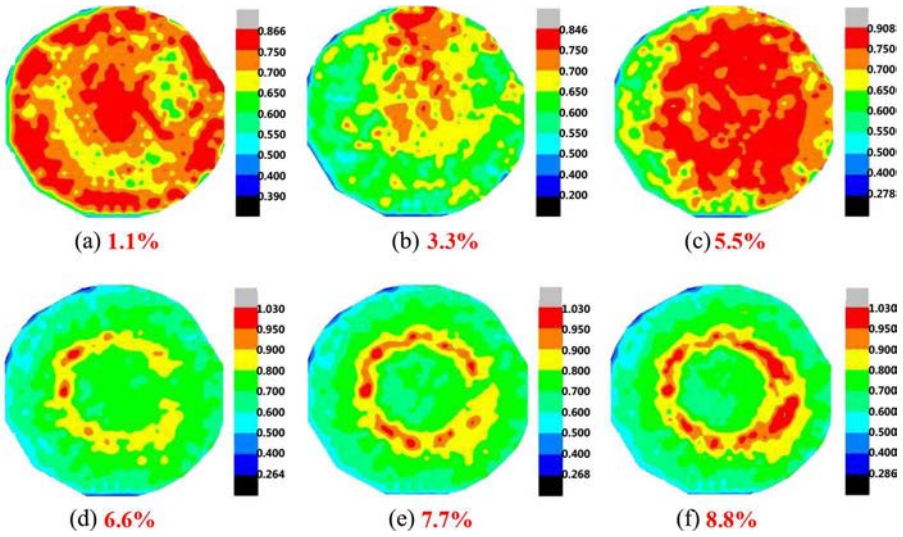

Figure 24. The effective strain distributions in the cross section (*z*-direction, the 1/4 height of particle sample) of granular assembly with increasing vertical displacements.

distributions along *x*-direction and *y*-direction in the vertical sections, respectively, and at different heights of the triaxial specimen in the transverse sections with increasing axial strains.

Figures 22 and 23 give the effective strain distributions along *x*-direction and *y*-direction in the vertical section of the triaxial specimen with increasing axial strains, respectively. It can be seen that two intersection shear bands develop distinctly after the axial strain of 5.5% and run through the triaxial specimen progressively in these two directions.

The effective strain distributions in the cross section along *z*-direction at the heights of 2/8*h*, 3/8*h*, 4/8*h*, 5/8*h*, and 6/8*h* (*h* is the height of the triaxial specimen) of the specimen are given in Figures 24–28, respectively. Also the changes of the effective strain distributions with increasing axial strains are given in each figure. It can be seen that the shear bands develop distinctly in different parts for different cross sections after the axial strain of 5.5%, namely the bigger circular ring in the upper cross section, then less and less circular ring down to the middle part and then bigger and bigger circular ring down to the bottom.

By comprehensive analysis of the effective strain distributions in the vertical sections and cross sections, an axial symmetric shear band like two hoppers stacking as the shape of rotational "X" in triaxial sample can be figured out, as is shown in Figure 29. It also can be concluded that the shear band starts to develop before the peak stress and that the deformation is mainly concentrated in an axial symmetric shear band like two hoppers stacking while the other parts of the specimen have little change.

It can be seen that different particle-generation methods result in different failure modes from the analysis above, which is mainly due to the difference of the boundary constraints. For the method of "step-by-step membrane-forming method," the contacts between the membrane particles and inner particles are a little weak, so that the constraint of the membrane boundary is also weak, and it is more deformable and easy to trigger the development of a single shear band. For the method of "once membrane-forming method," the contacts between the membrane particles and inner particles are very tight, so that the constraint of the membrane boundary is strong and the axial symmetric shear band is formed in the end.

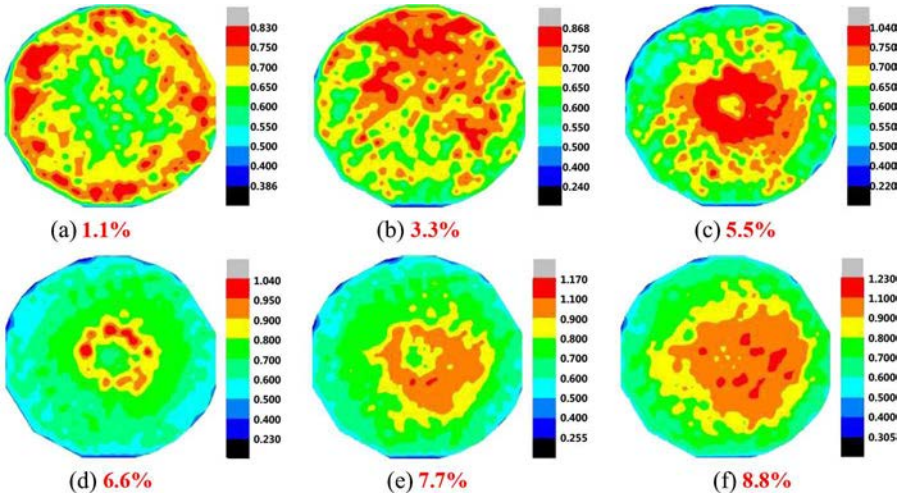

Figure 25. The effective strain distributions in the cross section (*z*-direction, the 3/8 height of particle sample) of granular assembly with increasing vertical displacements.

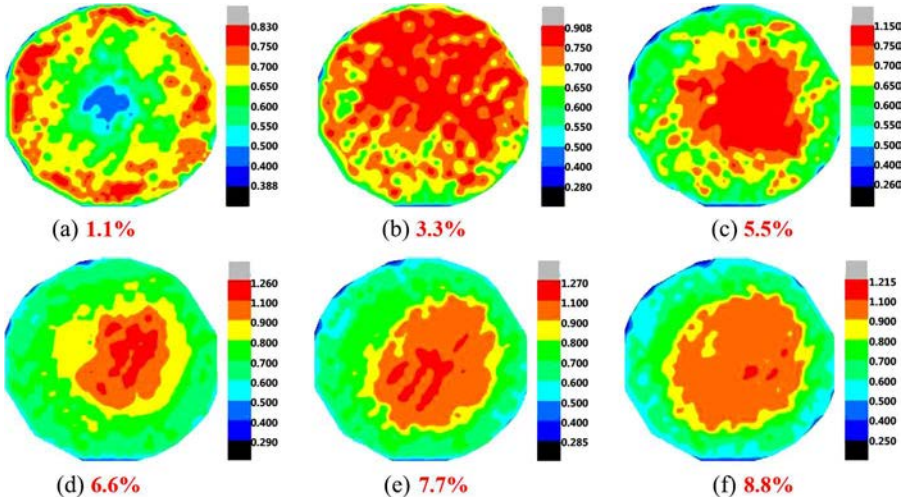

Figure 26. The effective strain distributions in the cross section (*z*-direction, the 1/2 height of particle sample) of granular assembly with increasing vertical displacements.

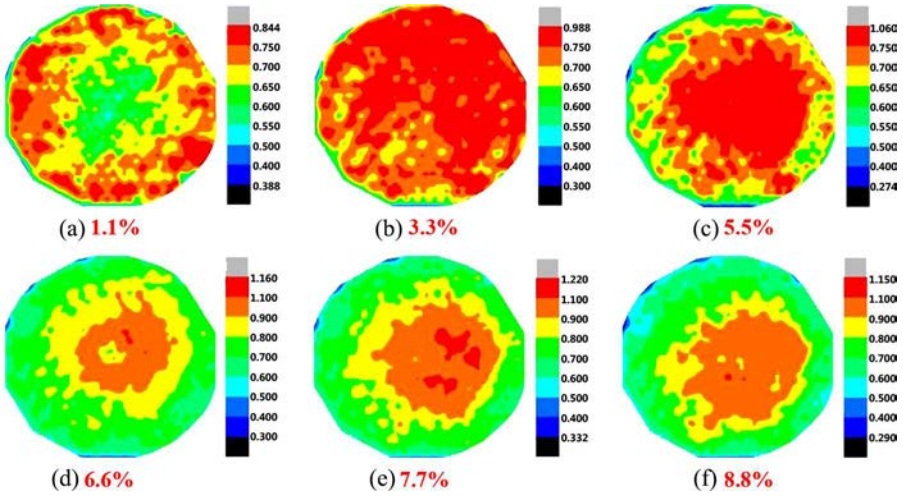

Figure 27. The effective strain distributions in the cross section (*z*-direction, the 5/8 height of particle sample) of granular assembly with increasing vertical displacements.

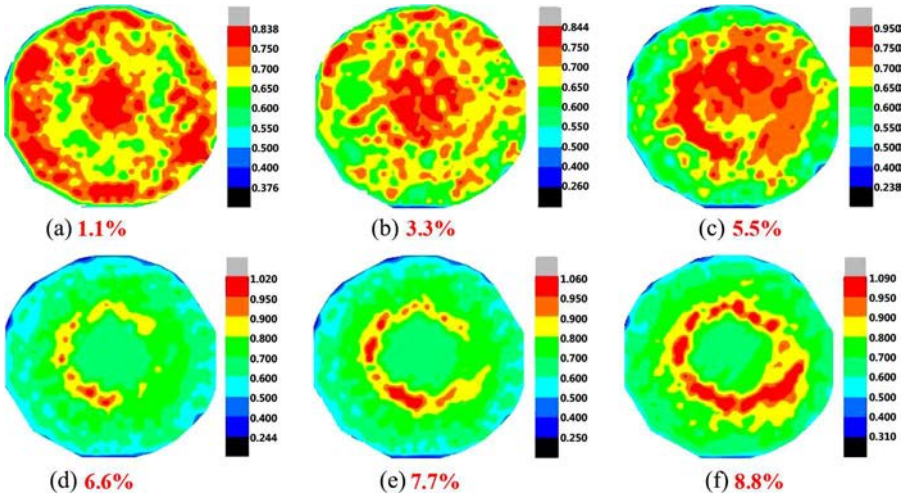

Figure 28. The effective strain distributions in the cross section (*z*-direction, the 3/4 height of particle sample) of granular assembly with increasing vertical displacements.

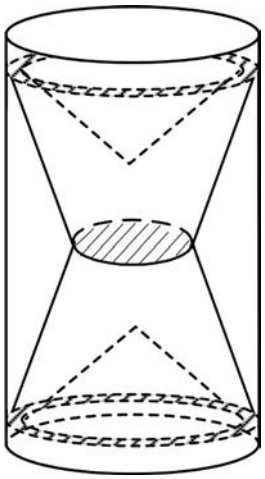

Figure 29. The outline of shear band in triaxial test.

Conclusion

Triaxial tests are applied widely to study the mechanical behaviors of granular materials. However, the shear bands during the failure process of granular materials are hardly observed in three dimensions. In this paper, the DEM is used to analyze the triaxial test of granular materials. The definition of the effective strain is presented to describe the macroscopic deformation process of granular material in three dimensions based on the locations and displacements of particles on micro-scale. To illustrate the mechanism of shear bands in DEM simulations, two different methods are adopted to generate the particles and the membrane for triaxial samples. The first is called the step-by-step membrane-forming method, which generates the internal particles first, then encloses the membrane around the particles; the second is called the once membrane-forming method, which generates the internal particles and the enclosed membrane simultaneously. With these two particle-generation methods, the effective strain distributions in longitudinal section and transverse section of the triaxial specimen are simulated with DEM to investigate the progressive failure and the evolution of the shear bands in three dimensions. Two different typical shear band failure modes are observed in triaxial tests under the sample generation methods accordingly. One is a single shear band like a scraper bowl which originates from the upper part then slants through the sample; the other is an axial symmetric shear band like two hoppers stacking as the shape of rotational "X" in triaxial specimen. During the generations of shear banks, the deformation of granular materials is mainly concentrated in the shear band. The generation mechanisms of the two shear bands are discussed.

Funding

This work was financially supported by the National Natural Science Fund of China (51138001, 51279025), the National Key Basic Research and Development Program (973 Program, 2010CB731502), and the Fundamental Research Funds for the Central Universities (DUT14LK20, DUT16ZD211).

References

Abe, S., G. H. Van, and J. L. Urai. 2011. DEM simulation of normal faults in cohesive materials. *Tectonophysics* 512:12–21. doi:10.1016/j.tecto.2011.09.008.

Al-Raoush, R. 2007. Microstructure characterization of granular materials. *Physical A* 377:545–58. doi:10.1016/j.physa.2006.11.090.

Alshibli, K. A., and A. Hasan. 2008. Spatial variation of void ratio and shear band thickness in sand using X-ray computed tomography. *Geotechnique* 58:249–57. doi:10.1680/geot.2008.58.4.249.

Alshibli, K. A., Sture, S., Costes, N. C., Frank, M. L., Lankton, M. R., Batiste, S. N., and Swanson, R. A. 2000. Assessment of localized deformations in sand using X-ray computed tomography. *Geotechnical Testing Journal* 23:274–99. doi:10.1520/gtj11051j.

Bagi, K. 1996. Stress and strain in granular assemblies. *Mechanics of Materials* 22:165–77. doi:10.1016/0167-6636(95)00044-5.

Belheine, N., J.-P. Plassiard, F.-V. Donze, F. Darve, and A. Seridi. 2009. Numerical simulation of drained triaxial test using 3D discrete element modeling. *Computers and Geotechnics* 36:320–331. doi:10.1016/j.compgeo.2008.02.003.

Borja, R. I., X. Y. Song, A. L. Rechenmacher, S. Abedi, and W. Wu. 2013. Shear band in sand with spatially varying density. *Journal of the Mechanics and Physics of Solids* 61:219–34. doi:10.1016/j.jmps.2012.07.008.

Chang, C. S., and A. Misra. 1988. Packing structure and mechanical properties of granulates. *Journal of Engineering Mechanics* 116:1077–93. doi:10.1061/(asce)0733-9399(1990)116:5(1077).

Christophe, S., G. Philippe, and V. Pascal. 2009. Influence of relative density on granular materials behavior: DEM simulations of triaxial tests. *Granular Matter* 11:221–36. doi:10.1007/s10035-009-0138-2.

Chupin, O., A. L. Rechenmacher, and S. Abedi. 2011. Finite strain analysis of nonuniform deformations inside shear bands in sands. *International Journal for Numerical and Analytical Methods in Geomechanics* 36:1651–66. doi:10.1002/nag.1071.

Cundall, P. A., and O. D. L. Strack. 1979. A discrete numerical model for granular assemblies. *Geotechnique* 29:47–65. doi:10.1680/geot.1979.29.1.47.

Desrues, J., J. Lanier, and P. Stutz. 1985. Localization of the deformation in tests on sand sample. *Engineering Fracture Mechanics* 21:909–921. doi:10.1016/0013-7944(85)90097-9.

Desrues, J., R. Chambon, M. Mokni, and F. Mazerolle. 1996. Void ratio evolution inside shear bands in triaxial sand specimens studied by computed tomography. *Geotechnique* 46:529–46. doi:10.1680/geot.1996.46.3.529.

Geraldine, C., and O. S. Catherine. 2008. Effective simulation of flexible lateral boundaries in two- and three-dimensional DEM simulations. *Particuology* 6:483–500. doi:10.1016/j.partic.2008.07.018.

Hall, S. A., M. Bornert, J. Desrues, Y. Pannier, N. Lenoir, G. Viggiani, and P. Bésuelle. 2010. Discrete and continuum analysis of localised deformation in sand using X-ray uCT and volumetric digital image correlation. *Geotechnique* 60:315–22. doi:10.1680/geot.2010.60.5.315.

Hare, C. L., and M. Ghadiri. 2013. Influence of measurement cell size on predicted attrition by the Distinct Element Method. *Powder Technology* 236:100–106. doi:10.1016/j.powtec.2012.04.061.

Kozicki, J., and F. V. Donze. 2009. Yade-open DEM: An open source software using a discrete element method to simulate granular material. *Engineering Computations* 26:786–805. doi:10.1108/02644400910985170.

Li, X. K. X. H. Chu, and Y. T. Feng. 2005. A discrete particle model and numerical modeling of the failure modes of granular materials. *Engineering Computations* 22:894–920. doi:10.1108/02644400510626479.

Liao, C. L., T. P. Chang, D. H. Young, and C. S. Chang. 1997. Stress-strain relationship for granular materials based on the hypothesis of best fit. *International Journal of Solids and Structures* 34:4087–4100. doi:10.1016/s0020-7683(97)00015-2.

Oda, M., and K. Iwashita. 1999. *Mechanics of granular materials*. Rotterdam: A. A. Ballkema.

Oda, M., and H. Kazama. 1998. Microstructure of shear bands and its relation to the mechanism of dilatancy and failure of dense granular soils. *Geotechnique* 48:465–81. doi:10.1680/geot.1998.48.4.465.

Oda, M., J. Konishi, and S. Nemat-Nasser. 1982. Experimental micromechanical evaluation of strength of granular materials: Effects of particular rolling. *Mechanics of Materials* 1:269–83. doi:10.1016/0167-6636(82)90027-8.

Oda, M., T. Takemura, and M. Takahashi. 2004. Microstructure in shear band observed by microfocus X-ray computed tomography. *Geotechnique* 54:539–42. doi:10.1680/geot.2004.54.8.539.

Rechenmacher, A. L., S. Abedi, and O. Chupin. 2010. Evolution of force chains in shear bands in sands. *Geotechnique* 60:343–51. doi:10.1680/geot.2010.60.5.343.

Rechenmacher, A. L., S. Abedi, O. Chupin, and A. D. Orlando. 2011. Characterization of mesoscale instabilities in localized granular shear using digital image correlation. *Acta Geotechnica* 6:205–217. doi:10.1007/s11440-011-0147-2.

Shao, L. T., Z. P. Wang, and G. C. Han. 2001. Digital image processing technique for measurement of the radial deformation of specimen in triaxial test. *Journal of Geotechnical Engineering* 23:337–41.

Sun, D. A., W. X. Huang, and Y. P. Yao. 2008. An experimental study of failure and softening in sand under three-dimensional stress condition. *Granular Matter* 10:187–95. doi:10.1007/s10035-008-0083-5.

Vardoulakis, I. 1980. Shear band inclination and shear modulus in biaxial tests. *International Journal for Numerical and Analytical Methods in Geomechanics* 4:103–119. doi:10.1002/nag.1610040202.

Zhang, D., and W. J. White. 1998. An efficient calculation method for particle motion in discrete element simulations. *Powder Technology* 98:223–30. doi:10.1016/s0032-5910(98)00055-2.

Zhao, X. H., and Q. H. Zhang. 2003. *Shear band tests and numerical analysis for soils*. Beijing: Mechanical Industry Press.